Acta Pharmaceutica Sinica B 2023;13(1):327−343

Chinese Pharmaceutical Association
Institute of Materia Medica, Chinese Academy of Medical Sciences

Acta Pharmaceutica Sinica B

www.elsevier.com/locate/apsb
www.sciencedirect.com

ORIGINAL ARTICLE

Macrophage-evading and tumor-specific apoptosis inducing nanoparticles for targeted cancer therapy

Zimo Liu[a,b,†], Xuefei Zhou[c,†], Qi Li[a], Youqing Shen[b], Tianhua Zhou[d,e], Xiangrui Liu[a,d,*]

[a]*Department of Pharmacology and Department of Gastroenterology of the Second Affiliated Hospital, Zhejiang University School of Medicine, Hangzhou 310058, China*
[b]*College of Chemical and Biological Engineering, Zhejiang University, Hangzhou 310027, China*
[c]*International Institutes of Medicine, The Fourth Affiliated Hospital of Zhejiang University School of Medicine, Yiwu 322000, China*
[d]*Cancer Center, Zhejiang University, Hangzhou 310058, China*
[e]*Department of Cell Biology, School of Medicine, Zhejiang University, Hangzhou 310058, China*

Received 24 February 2022; received in revised form 29 March 2022; accepted 8 April 2022

KEY WORDS

TRAIL;
Fibroblast;
Nanoparticles;
Mononuclear phagocyte system;
Membrane coating;
Chloroquine;
Cancer therapy;
Drug delivery

Abstract Extended circulation of anticancer nanodrugs in blood stream is essential for their clinical applications. However, administered nanoparticles are rapidly sequestered and cleared by cells of the mononuclear phagocyte system (MPS). In this study, we developed a biomimetic nanosystem that is able to efficiently escape MPS and target tumor tissues. The fabricated nanoparticles (TM-CQ/NPs) were coated with fibroblast cell membrane expressing tumor necrosis factor (TNF)-related apoptosis inducing ligand (TRAIL). Coating with this functionalized membrane reduced the endocytosis of nanoparticles by macrophages, but increased the nanoparticle uptake in tumor cells. Importantly, this membrane coating specifically induced tumor cell apoptosis *via* the interaction of TRAIL and its cognate death receptors. Meanwhile, the encapsulated chloroquine (CQ) further suppressed the uptake of nanoparticles by macrophages, and synergized with TRAIL to induce tumor cell apoptosis. The vigorous antitumor efficacy in two mice tumor models confirmed our nanosystem was an effective approach to address the MPS challenge for cancer therapy. Together, our TM-CQ/NPs nanosystem provides a feasible approach to precisely target tumor tissues and improve anticancer efficacy.

*Corresponding author. Tel.: +86 15967155397.
E-mail address: xiangrui@zju.edu.cn (Xiangrui Liu).
†These authors made equal contributions to this work.
Peer review under responsibility of Chinese Pharmaceutical Association and Institute of Materia Medica, Chinese Academy of Medical Sciences.

https://doi.org/10.1016/j.apsb.2022.05.010

1. Introduction

In the past decade, nanodrugs have shown considerable advances for cancer therapy[1−3]. However, despite the successful application of several nano-formulations, such as Doxil and Abraxane, most nanodrugs failed for clinical translation due to their insufficient tumor accumulation, and consequently, compromised anticancer efficacy[4,5]. The mononuclear phagocyte system (MPS), formed by resident macrophages in the liver and spleen, has been demonstrated to sequester the majority of administered nanoparticles, leading to impeded delivery of therapeutics to the tumor site and even systemic toxicity[6−8]. To evade the fast clearance of nanoparticles by macrophages, multiple strategies have been proposed to engineer stealth nanoparticles[9,10], the most notable being pegylation by introducing polyethylene glycol (PEG) on nanoparticle surfaces[11,12]. Nonetheless, pegylation inevitably reduces tumor cell uptake, combined with potential side effects induced by over-injection of pegylated nanoparticles[13]. Therefore, development of effective and safe methods to escape the MPS clearance is critical for the clinical translation of nanodrugs.

Biomimetic nanoparticles based on cell membrane-coating technique have emerged as a novel platform for drug delivery, providing new opportunities to address the MPS challenge for prolonged circulation of injected nanoparticles[14−16]. Basically, the coated cell membrane presents CD47 or other complement regulators to protect the nanoparticles from phagocytosis and subsequent clearance by the MPS[17,18]. Further, cell membrane-coated nanoparticles tend to mimic the properties of the source cells for acquiring additional functions, such as homologous targeting[19,20]. To date, numerous cell membranes have been investigated for the development of nanotherapeutics to bypass macrophage uptake and clearance[21]. For instance, nanoparticles coated with red blood cell (RBC) membrane displayed extended systemic circulation in preclinical studies[14,22,23]. However, these membranes are only designed to improve the circulation or targeting effect of nanoparticles without direct therapeutic functions.

Considering the enhanced potential of nanoparticles to accumulate in the tumor tissue by membrane coating, the functionalization of cell membrane with the expression of therapeutic proteins may generate potent anticancer effect. Tumor necrosis factor (TNF)-related apoptosis inducing ligand (TRAIL) serves as a promising therapeutic protein, which selectively induces tumor cell apoptosis by binding to its cognate death receptor DR4 or DR5 overexpressed on the surface of tumor cells[24,25]. Nevertheless, the clinical application of recombinant TRAIL has been limited by its short circulation half-life, inefficient tumor accumulation[26], and potential hepatotoxicity[27,28] induced by the non-targeted distribution of administered TRAIL in the liver. Our previous investigation[29−32] has demonstrated that TRAIL expressed by tumor-associated fibroblasts induced apoptosis of neighboring tumor cells. Importantly, fibroblast membrane-coated nanoparticles have the potential to target tumor sites with the presentation of adhesion proteins[33,34]. Thus, biomimetic nanoparticles coated with TRAIL-expressing fibroblast membrane could be an ideal candidate for tumor ablation, while simultaneously overcoming the delivery obstacles for both uncoated nanoparticles and TRAIL protein.

Of note, most strategies for overcoming the MPS barrier rely on the surface modification of nanoparticles to decrease the interaction with macrophages, with little emphasis placed on resident macrophage modulation to reduce nanoparticle internalization[35,36]. Chloroquine (CQ), a clinically approved antimalarial agent and autophagy inhibitor, has been shown to specifically reduce nanoparticle uptake in macrophages[37,38], providing an alternative for addressing this barrier. However, the non-specific distribution and the dose-related side effect restrict its further application in clinic.

In this study, we find that LX2 (human hepatic stellate cells) membrane-coated nanoparticles (M-NPs) showed improved blood circulation compared with non-coated poly lactic-*co*-glycolic acid (PLGA) nanoparticles (NPs), while CQ further inhibited the MPS uptake and significantly improved the accumulation of M-NPs in tumors. In addition, we stably expressed the tumor specific apoptotic protein TRAIL on the membrane of LX2 cells, and found CQ could further improve the apoptotic effect of TRAIL in tumor cells. Based on these findings, we developed CQ-encapsulated NPs, which were coated with TRAIL-expressing fibroblast membrane, named TM-CQ/NPs (see Scheme 1). This nanosystem presented dramatic antitumor activity in both orthotopic liver and intraperitoneal tumor models, indicating the therapeutic potential of our macrophage-evading and tumor-targeted cancer therapeutic strategy.

2. Materials and methods

2.1. Materials

Poly (D,L-lactic-*co*-glycolic acid) (lactide:glycolide 75:25 PLGA, MW 4000−15,000 Da), chloroquine (CQ), poly (vinyl alcohol) (PVA, MW 13,000−23,000) and Rhodamine B (83689) were purchased from Sigma−Aldrich (St. Louis, MO, USA). 1,1′-Dioctadecyltetramethyl indotricarbocyanine iodide (DiR, 125964, PerkinElmer, Shanghai, China) was bought from PerkinElmer.

2.2. Cell lines and animals

The human hepatic stellate cell line LX2 and human hepatocarcinoma cell line Huh7 were kindly provided by Dr. Yanning Liu (The First Affiliated Hospital, Zhejiang University School of Medicine, Hangzhou, China). The murine ascites macrophage cell line RAW264.7 and murine colon carcinoma cell line CT26 were purchased from American Type Culture Collection (ATCC, Rockefeller, MA, USA). LX2, Huh7 and RAW264.7 were maintained in glucose Dulbecco's modified Eagle Medium (DMEM, Gibco, Grand Island, CA, USA) supplemented with 10% fetal bovine serum (FBS, Gibco), 100 units/mL penicillin, and 100 units/mL streptomycin. CT26 cells were cultured in RPMI 1640

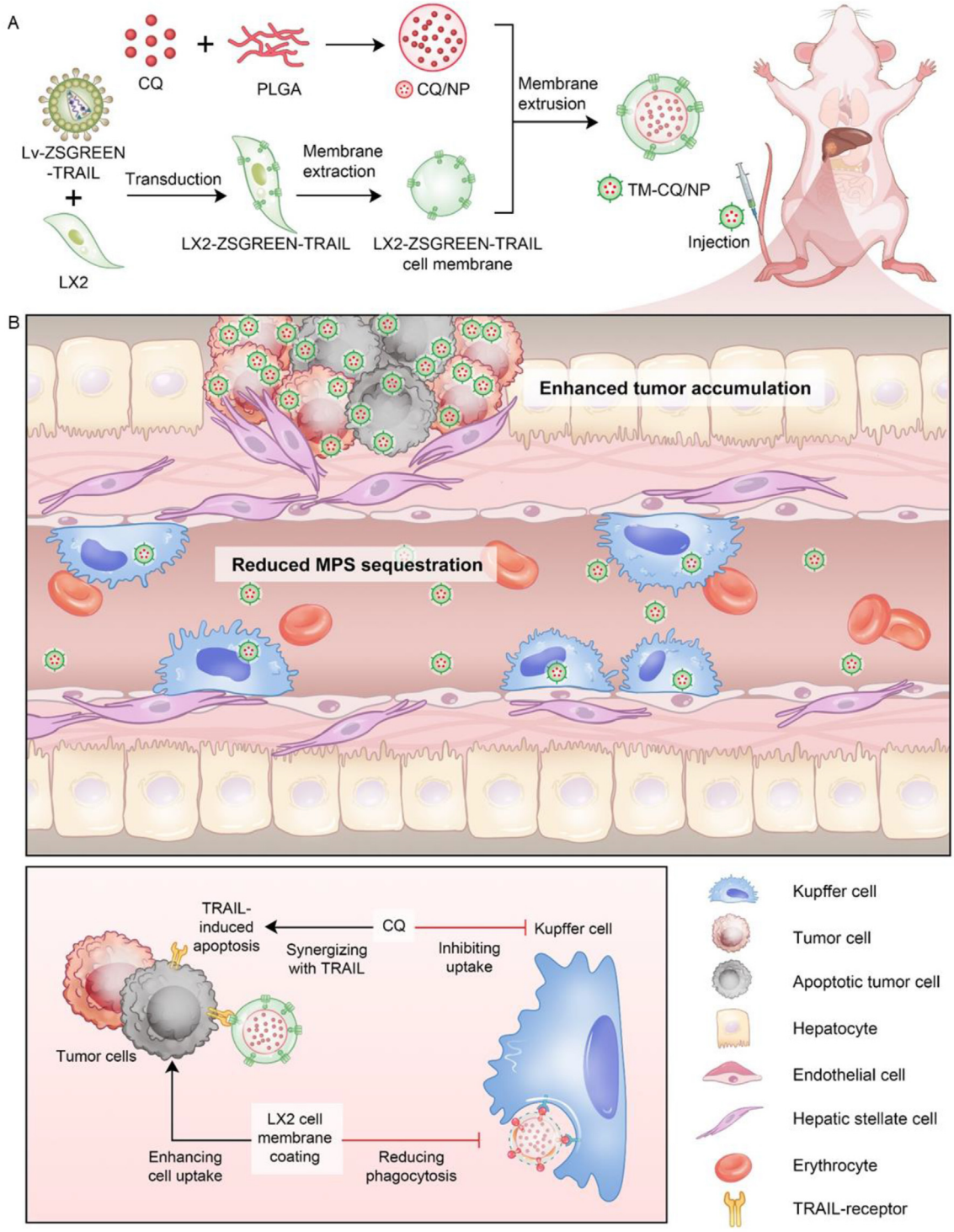

Scheme 1 Schematic of the preparation of TM-CQ/NPs for macrophage-evading and effective cancer therapy. (A) Fabrication of TM-CQ/NPs. Firstly, CQ/NPs were prepared by single-emulsion. Then, lentivirus vector of TRAIL(Lv-TRAIL-ZSGREEN) was constructed and LX2 cells were transfected to stably express TRAIL-ZSGREEN. TRAIL-ZSGREEN-expressing LX2 cell membrane was extracted from LX2-TRAIL-ZSGREEN cells by sonication and super-centrifugation. Finally, TM-CQ/NPs was fabricated by extruding LX2-TRAIL-ZSGREEN cell membrane onto the CQ/NPs. (B) Circulating nanoparticles encountered the MPS and most of them were sequestrated in Kupffer cells. TM-CQ/NPs showed reduced Kupffer cell uptakes and enhanced tumor accumulations. CQ not only inhibited the uptake of membrane-coated nanoparticles in Kupffer cell, but also synergized with TRAIL to induce apoptosis of tumor cells.

(Gibco) with 10% FBS (Gibco). All the cell lines were cultured at 37 °C in a humidified incubator with an atmosphere of 5% CO2.

All animal experiments were approved by Zhejiang University Experimental Animal Welfare and Ethics Committee under Institutional Animal Care and Use Committee guidelines. Female ICR strain mice, BALB/c mice and BALB/c athymic mice (6−8 weeks old) were housed and maintained in accordance with the institutional guidelines of the Zhejiang Academy of Medical Science.

2.3. Liver perfusion and isolation of Kupffer cells

The experiment was performed according to the manufacturer's protocol. Briefly, BALB/c nude mice or ICR mice were anesthetized with a 16G catheter inserted into the portal vein, followed by the liver perfused with warm D-Hank's buffer. Once the liver began to blanch, the inferior vena cava was quickly cut to allow outflow of blood and relieve pressure in the liver. The solution was then changed to D-Hank's buffer with collagenase type IV. The perfused liver was slowly taken out and placed in ice-cold D-Hank's buffer. Solid parts of the liver were discarded after the cell suspension was filtered through a 100 μm sterile cell strainer. The filtered cells were centrifuged, the cloudy supernatant (containing liver non-parenchymal cells) and the precipitation (containing liver parenchymal cells) were separated. Parenchymal and non-parenchymal cells were washed three times and resuspended with MACS buffer (#130-091-376 and #130-091-222, Miltenyi, Bergisch Gladbach, Germany). The non-parenchymal cells were incubated with anti-F4/80 MicroBeads (#130-110-443, Miltenyi) and mixed gently. After refrigerated for 10 min at 4 °C, the non-parenchymal cells were proceeded to magnetic separation with LS Columns (Miltenyi) according to the manual. The magnetically labeled Kupffer cells were flushed out of the column, as the column was moved from the magnetic field of MACS Separator (Miltenyi). Kupffer cells were seeded to confocal dishes or 12-well plates and maintained in DMEM supplemented with 10% FBS.

2.4. Generation and characterization of TRAIL-ZSGREEN overexpressing cell line

To establish the cell line stably expressing TRAIL-ZSGREEN fusion protein, LX2 cells were transfected with a lentivirus vector that expresses TRAIL-ZSGREEN and further screened with G418. TRAIL expression on the LX2-TRAIL-ZSGREEN cell membrane was then analyzed by immunoblotting analysis and flow cytometry.

2.5. Preparation of cell membrane nanovesicles

LX2 cells were harvested and washed with cold phosphate buffered saline (PBS) for three times. Then, the cells were suspended in a hypotonic lysing buffer (pH7.4) containing 1 × phenylmethylsulfonyl fluoride (PMSF, 36978, Thermo Fisher, Waltham, MA, USA) and phosphatase inhibitor cocktail (78420, Thermo Fisher). Cells were lysed on a shaker at 4 °C for 4 h. Cell lysate solution was centrifuged at 1000×*g* for 10 min at 4 °C three times and the pellet was discarded. Then the supernatant solution was centrifuged at 10,000×*g* for another 30 min with pellet discarded. The supernatant was further centrifuged at 100,000×*g* for 60 min at 4 °C to collect the pellet. To prepare cell membrane nanovesicles, the obtained cell membrane suspended in PBS were then passed through a Mini-Extruder (Avanti Polar Lipids, Birmingham, AL, USA) with 0.2 μm polycarbonate porous membrane (Whatman, Maidstone, England) to produce uniform nanovesicles. Membrane protein concentration was quantified by BCA protein assay kit (Beyotime Biotechnology, Shanghai, China).

2.6. Preparation and characterization of membrane-coated NPs

PLGA nanoparticles (NPs) were prepared according to a published method with modifications[39−41]. Briefly, PLGA was dissolved in dichloromethane to 10 mg/mL. The solution was added dropwise to 3 mL of deionized water. The mixture was then stirred at room temperature for 4 h. The resulting nanoparticles were washed with deionized water for three times. For the preparation of CQ/NPs, 200 mg PLGA and 20 mg CQ were dissolved in 20 mL dichloromethane and sonicated until they were completely dissolved. After that, the organic solution was added to 20 mL PVA solution (4%, *w*/*v*) with sonication for 5 min to form emulsion. Then, the obtained emulsion was added dropwise into 200 mL PVA solution (1%, *w*/*v*), while the solution was homogenized with a homogenizer (IKA, Staufen, Germany). The hardened particles were centrifuged at 9000 rpm for 30 min (Pico17, Thermo Fisher, Waltham, MA, USA) and washed three times with deionized water. For *in vitro* cell uptake studies, Rhodamine B was loaded into nanoparticles at a content of 0.4% (*w*/*w*). Briefly, 10 mg PLGA and 40 μg Rhodamine B were dissolved in 2 mL dichloromethane. The organic solution was added to 10 mL PVA solution (1%, *w*/*v*) with sonication for 5 min to form emulsion. The emulsion was then stirred at room temperature for 4 h. The obtained nanoparticles were washed with deionized water for three times. For *in vivo* biodistribution studies, DiR with a 748 nm excitation/780 emission fluorescence profile was loaded into nanoparticles at a content of 2% (*w*/*w*). Briefly, 10 mg PLGA and 200 μg DiR were dissolved in 2 mL dichloromethane. Then, the solution was added dropwise to 10 mL PVA solution (1%, *w*/*v*) with sonication for 5 min to form emulsion. After stirring at room temperature for 4 h, DiR/NPs were washed with deionized water. PLGA nanoparticles were coated with cell membrane nanovesicles *via* extrusion through a 0.2 μm polycarbonate porous membrane using a Mini-Extruder.

The size and distribution of nanoparticles were measured by dynamic light scattering (DLS) on a Zetasizer Nano ZS particle sizer (3600, Malvern Instruments Ltd., Malvern, England). The morphology images of the cell membrane nanovesicles, PLGA nanoparticles, and membrane-coated nanoparticles were recorded using a transmission electron microscope (TEM, JEOL JEM-1010, Hitachi, Tokyo, Japan) with phosphotungstic acid. CQ/NPs were dissolved in methyl alcohol and ultrasonized for 20 s. The EP tube containing dissolved CQ/NPs was placed in the fume hood overnight to evaporate the solvent. Then, methyl alcohol was added to dissolve CQ fully. The dispersion was centrifuged at 13,500 rpm for 10 min at 4 °C (Pico17, Thermo Fisher). The supernatant was collected to analyze the concentration of CQ by HPLC. The drug encapsulation efficiency (EE) is defined as the weight percentage of CQ in CQ/NPs compared to the initial feeding amount of CQ. The drug loading efficiency (DLE) is calculated from the mass of incorporated CQ divided by the weight of CQ/NPs.

2.7. Crystal violet assay

CT26, Huh7, and RAW264.7 cells were treated with M-NPs, TM-NPs, CQ/NPs or TM-CQ/NPs nanoparticles after 24 h of plating. Nanoparticles were dissolved in PBS and added to cells at a final PLGA concentration of 180 μg/mL or membrane protein

concentration of 16.7 mg/mL. Cell viability was determined after 24 h of treatment. Viable cells were stained with crystal violet and images were obtained by a digital camera (EX30, Sunny intelligent technology, Ningbo, China).

2.8. Protein expression analyses

Cells were treated with TM-NPs, CQ/NPs or TM-CQ/NPs nanoparticles for 24 h at the concentration mentioned in crystal violet assay. Cells were lysed and the resulting lysates were centrifuged at 10,000 rpm for 10 min at 4 °C (Pico17, Thermo Fisher). The supernatants were collected and the protein concentration was quantified and normalized by BCA protein assay. Proteins were separated on 10% SDS-PAGE (P0455M, Beyotime, Shanghai, China), and transferred to PVDF membranes (EMD Millipore, Billerica, MA, USA). The membranes were blocked with 5% BSA for 1 h and immunoblotted with antibodies against TRAIL (ab10516, 1: 1000 dilution, *v/v*, Abcam, Cambridge, UK), β-tubulin (AF5012, 1: 5000 dilution, *v/v*, Beyotime, Shanghai, China), Na^+/K^+ ATPase (A01483, 1: 1000 dilution, *v/v*, GenScript, Nanjing, China), PARP (#9532, 1:1000 dilution, *v/v*, Cell signaling Danvers, MA, USA), cleaved-PARP (#5625, 1:1000 dilution, *v/v*, Cell signaling Danvers) or GAPDH (ab8245, 1:5000 dilution, *v/v*, Abcam). Following incubation with the secondary antibodies, proteins were visualized with enhanced chemiluminescence reagent (P0018S, Beyotime, Shanghai, China).

2.9. Cellular internalization

For confocal microscopy detection, cells in 1 mL of growth medium were seeded onto glass-bottom dishes at the density of 1×10^5 cells per well. Huh7 and LX2 cells were incubated with Rhodamine B-labeled NPs or M-NPs at the concentration of 100 μg/mL. RAW264.7 and Kupffer cells were incubated with nanoparticles at the concentration of 10 μg/mL. For CQ pretreated groups, Huh7 and Kupffer cells were first treated with 50 μmol/L of chloroquine for 24 h before the addition of nanoparticles. At certain time points (10 min and 6 h), the medium was discarded and the cells were washed three times with PBS. Cells were visualized with confocal microscopy after incubated with Hoechst 33342 for 20 min. For flow cytometric assay, cells were seeded in 12-well plates at a density of 5×10^5 cells/well and cultured for 24 h in 2 mL of DMEM containing 10% FBS. Then the experiments were carried out in the same conditions as confocal imaging. At timed intervals, cells were washed with PBS and digested by trypsin, and then centrifuged at 1000 rpm for 3 min (Pico17, Thermo Fisher) to remove the trypsin. The collected cells were resuspended in 0.5 mL PBS and cellular uptake was examined by flow cytometry (FACSCalibur, Becton Dickinson, Franklin Lakes, NJ, USA). Every 10,000 cells were counted to determine Rhodamine B-positive cells at the FL2 channel. FlowJo software was used for analysis.

2.10. Effects of endocytosis inhibitors on cellular uptake of nanoparticles

The cellular uptake of Rhodamine B-labeled NPs or M-NPs by Huh7, LX2 and Kupffer cells was analyzed by flow cytometry. Cells were grown in a 12-well plate at a density of 5×10^5 cells per well for 12 h. Cells were pretreated with cytochalasin D (5 μmol/L), chlorpromazine (30 μmol/L), chloroquine (50 μmol/L), filipin (7.5 μmol/L) or wortmannin (5 μmol/L) for 1 h following the addition of Rhodamine B-labelled nanoparticles (100 μg/mL) for further incubation. The Rhodamine B-positive cells were analyzed by flow cytometry at different time intervals and the results were analyzed using Flowjo software.

2.11. Blood clearance and biodistribution of nanoparticles

Female ICR mice were randomly grouped. For the chloroquine treated group, a dose of 40 mg/kg/day chloroquine phosphate with intraperitoneal injection over 3 days was used before the biodistribution studies. DiR-labeled NPs and M-NPs (10 mg/mL, 200 μL) were injected intravenously. At timed intervals, blood and major organs were collected and the fluorescence was detected by an IVIS imaging system (PerkinElmer, Shanghai, China). The excitation and emission wavelengths were set to 710 and 760 nm, respectively.

2.12. Anti-tumor study

For anti-tumor study in CT26 intraperitoneal mouse model, BALB/c mice were intraperitoneally inoculated with CT26 cells stably expressing luciferase (1×10^6 cells). After two weeks, the tumor-bearing mice were randomly divided into 4 groups ($n = 3$). Mice received four intraperitoneal injections of PBS, TM-NPs, CQ/NPs or TM-CQ/NPs as scheduled. For TM-NPs, CQ/NPs and TM-CQ/NPs-treated groups, an equivalent dose of CQ (20 mg/kg) or cell membrane vesicles was used. *In vivo* luciferase bioluminescence was monitored every 3 days with IVIS. D-Luciferin in 100 μL PBS was intraperitoneal injected and after 5 min the mice were imaged. Body weights were recorded on Days 0, 4, 7, 10 and 13. Mice were sacrificed on Day 13. Tumors were excised and weighed.

For anti-tumor study in Huh7 orthotopic tumor model, Huh7 cells stably expressing luciferase (2×10^6 cells) were injected into the right liver lobe in BALB/c athymic nude mice. To be specific, a subcostal incision was made on skin and peritoneum to expose the liver. The liver lobe was inoculated with cells in chilled matrigel solution (matrigel:PBS = 1:1, *v/v*, 356234 Becton Dickinson) using an insulin syringe (31 G, Becton Dickinson). The peritoneum and external skin were closed with an absorbable 6−0 suture with a continuous stitch. After two weeks of inoculation, grouped mice ($n = 7$ or 8) were treated with PBS, TM-NPs, CQ/NPs or TM-CQ/NPs through i.v. injection as scheduled. For TM-NPs, CQ/NPs and TM-CQ/NPs-treated groups, equivalent dose of CQ (20 mg/kg) or cell membrane vesicles was used. Bioluminescence imaging was used to monitor the tumor growth and the body weight in each group was recorded along with the treatment. Mice were sacrificed on Day 15. Tumor tissue and major organs (heart, liver, spleen, lung and kidney) were harvested for histological examinations. Long-term survival was also conducted on mice bearing Huh7 orthotopic tumors with different treatments ($n = 4$ or 5).

2.13. Nanoparticle accumulation in CT26 intraperitoneal tumor

For the chloroquine pretreated group, a dose of 40 mg/kg/day chloroquine phosphate was intraperitoneally injected over 7 days. BALB/c mice were intraperitoneal inoculated with CT26 tumor cells (1×10^6 cells). *In vivo* distribution studies were performed two weeks after inoculation. DiR-labeled NPs or M-NPs (10 mg/mL, $n = 5$) was injected into the tumor-bearing mice by intraperitoneal injection. Then, mice were sacrificed at 6 h. Tumors in abdominal

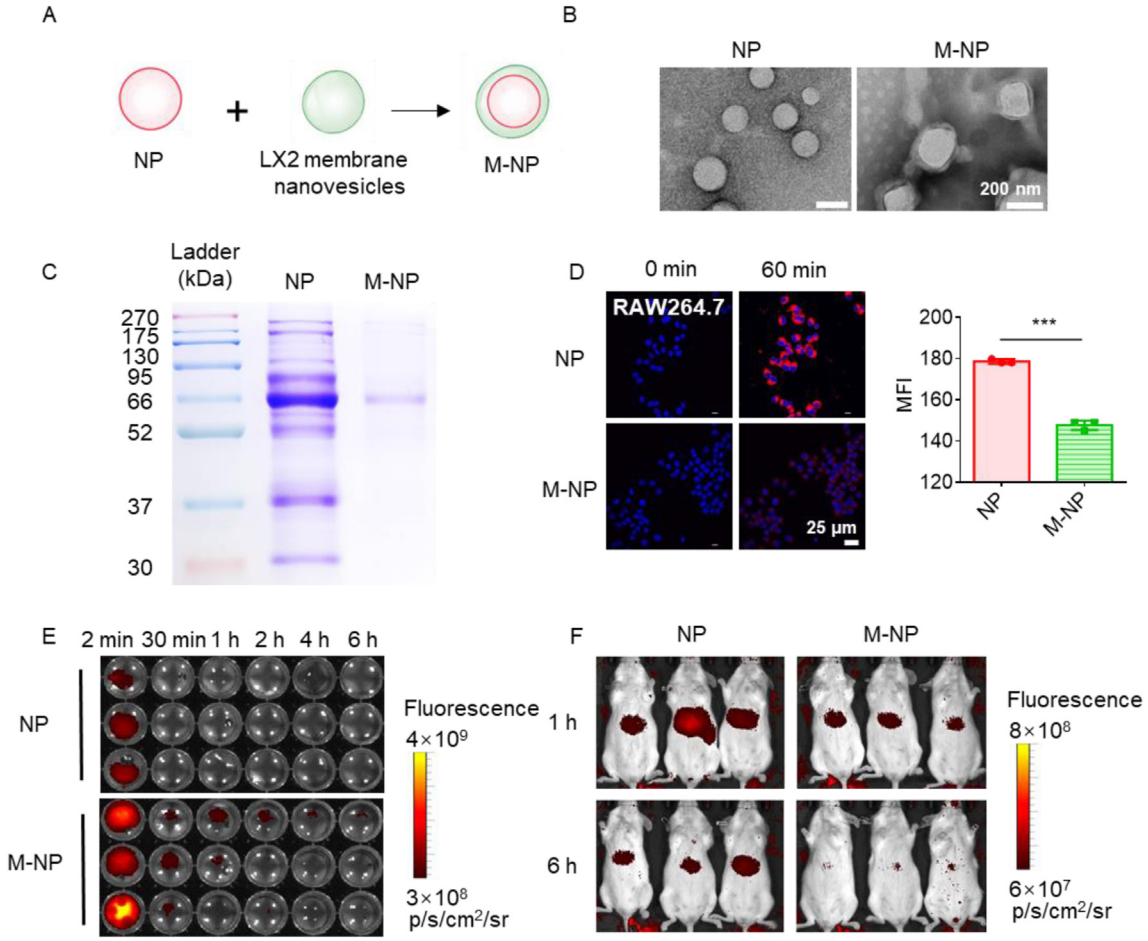

Figure 1 LX2 membrane-coated PLGA nanoparticles (M-NPs) showed decreased endocytosis in macrophages and improved blood circulation. (A) Schematic illustration of the fabrication of M-NPs. The LX2 cell membrane was isolated for PLGA nanoparticle (NP) coating to form M-NPs. (B) TEM images of NPs and M-NPs. Both were stained with phosphotungstic acid. Scale bar = 200 nm. (C) Detection of protein corona on NPs and M-NPs by SDS-PAGE. (D) *In vitro* cell uptake of NPs and M-NPs in RAW264.7 macrophages detected by confocal microscopy and flow cytometry. Confocal microscopy images were acquired after the cells were incubated with NPs or M-NPs for 1 h. The red fluorescence indicated Rhodamine B-labeled nanoparticles, and cell nuclei (blue) were stained with Hochest33342. Scale bar = 25 μm. The mean fluorescence intensity (MFI) in the cells was also quantitatively analyzed by flow cytometry at 1 h of the addition of nanoparticles. A total of 10,000 cells were counted per TRAIL and data are presented as the mean ± SD (n = 3). (E) *In vivo* blood circulation analysis of NPs or M-NPs in ICR mice (n = 3). At each timed interval, blood samples were collected from the orbit venous plexus and placed in a 96-well black plate for IVIS imaging. (F) Non-specific accumulation of NPs and M-NPs in the liver after 6 h of intravenous administration *via* the tail vein (n = 3).

cavity were excised, washed and homogenized. Fluorescence signals were recorded using IVIS.

2.14. *In vivo nanoparticles distribution in hepatic cell populations in Huh7 orthotopic tumor model*

Two weeks after tumor cell inoculation, the Huh7 tumor-bearing mice were used for nanoparticle distribution analysis. For the chloroquine pretreated group, chloroquine phosphate at a dose of 40 mg/kg/day was intraperitoneally injected for 3 continuous days. *In vivo* distribution studies were performed with i.v. injection of Rhodamine B-labeled nanoparticles (10 mg/mL, n = 5). Mice were anesthetized for abdominal incision. Then, the liver was perfused and parenchyma cells and non-parenchyma cells fractions were separated through centrifugation at 50×g for 5 min at 4 °C. Cells were resuspended with MACS buffer and mixed with each Miltenyi MicroBeads (#130-110-187 or #130-110-443, Miltenyi) and mixed gently. Parenchyma cells and non-parenchyma cells were proceeded to magnetic separation according to the manual. Therefore, parenchyma cells were divided into tumor cells and other parenchymal cells. Non-parenchyma cells were divided into Kupffer cells and other non-parenchymal cells. For flow cytometry, Rhodamine B positive events were detected with a 488 nm wavelength laser and a 585/42 optical filter. Gating strategy for nanoparticle positive events was set based on the nanoparticle untreated group.

2.15. *Safety evaluation*

ICR mice were randomly divided into four groups (n = 5) and received various treatments. Two important hepatic indicators (ALT: alanine aminotransferase, AST: aspartate aminotransferase) and BUN for kidney functions (blood urea nitrogen) were analyzed using a blood biochemical autoanalyzer (TEK8500 VET, TECOM, Nanchang, Jiangxi, China).

2.16. Nanoparticle protein corona analysis

CQ/NPs or TM-CQ/NPs were added to 1 mL of 10% mouse serum in PBS, rapidly mixed, and incubated at 37 °C for 6 h. Particles were washed with PBS to remove unbound proteins. After washing, the pellet was resuspended under shaking at 1200 rpm (Pico17, Thermo Fisher) in 50 μL reducing loading buffer overnight to desorb the proteins from the NPs surface. Hereafter, the samples were centrifuged again and 20 μL of each sample was reserved for SDS-PAGE electrophoresis. The resulting gel was fixed (79% water, 1% orthophosphoric acid, 20% methanol), and stained with a Coomassie Brilliant Blue R-250 solution overnight. The destained gel image was recorded.

2.17. Statistics and reproducibility

Statistical analyses were performed by two-tailed Student's *t*-test (two groups) or Analysis of Variance (ANOVA) (more than two groups) applying GraphPad Prism v7.03 software (Graphpad, San Diego, CA, USA). The data are expressed as mean ± SD. For all experiments, statistical difference was considered to be significant if P value was less than 0.05 ($^{*}P < 0.05$, $^{**}P < 0.01$, $^{***}P < 0.001$). Graphs were generated with GraphPad Prism v7.03 software or Microsoft Office Professional Plus 2016 (Microsoft, Redmond, WA, USA). All measurements were taken from distinct samples. Cultures of cell lines, mice (of matched age) and tumor samples were randomly allocated to the experiments. Collection of animal samples was not performed with blinding, but identical liver and tumor samples were used for further investigation.

3. Results and discussion

3.1. LX2 cell membrane coating improved the blood circulation of PLGA nanoparticles

Particle size and surface modifications have impact on the opsonin adsorption of nanomaterials and subsequent phagocytosis, which can further affect the blood circulation of nanoparticles[42–45]. In this study, we used PLGA, an US Food and Drug Administration (FDA)-approved co-polymer, as a model to fabricate nanoparticles with different sizes to investigate the optimal particle size for long blood circulation. PLGA nanoparticles were referred to as NPs. As shown in Supporting Information Fig. S1A, the sizes of three nanoparticles measured by dynamic light scattering (DLS) were 130, 180 and 350 nm, respectively. Besides, transmission electron microscopy (TEM) images showed spherical structure with similar morphology (Fig. S1A). To investigate the blood circulation of these nanoparticles, NPs were first labeled with a fluorescent dye 1,1′-dioctadecyl-3,3,3′,3′-tetramethylindotricarbo-cyanine iodide (DiR) *via* physical encapsulation (Fig. S1B). Blood circulation time was then measured by intravenously injecting the nanoparticles into mice and detecting the fluorescence intensity of DiR in the blood at certain time intervals. As shown in Figs. S1C and D, blood was collected at 2, 30 min, 1, 2, 4 and 6 h after particle administration to evaluate systemic nanoparticle concentration. Fig. S1D showed that the blood circulation half-life of NPs of 350 nm was 1.93 h, which was dramatically shorter than that of NPs of 130 nm (2.85 h) and 180 nm (2.47 h). These observations are consistent with previous reports[42,46]. PLGA nanoparticles of 130 and 180 nm presented comparable blood circulation. Considering the potential of increased drug loading for larger NPs[47,48], we chose 180 nm NPs for further studies.

The circulation time of nanoparticles with a designated size can be further impacted by their surface modifications[49]. Cell membrane coating has been demonstrated to be one of the strategies to camouflage the nanoparticles for prolonged blood circulation [50]. Here, we prepared cell membrane nanovesicles from human hepatic stellate cells (LX2) for PLGA nanoparticle coating to further improve their blood circulation. LX2 cells are activated fibroblasts, expressing surface protein N-cadherin[33,51], for the heterotypic adhesion with tumor cells. This property could make LX2-membrane-coated NPs (M-NPs) target tumor sites homogeneously[20] and heterogeneously. To prepare the M-NPs, LX2 membrane was first extracted and purified, followed by membrane-particle fusion *via* extrusion (Fig. 1A). To characterize the M-NPs, the particles were visualized with TEM after uranyl acetate staining. The acquired images showed a typical core shell structure with spherical morphology and the size was approximately 200 nm, indicating successful cell membrane coating around the PLGA cores (Fig. 1B).

To investigate the protein adsorption of NPs and M-NPs, particles were exposed to fetal bovine serum (FBS) and adsorbed proteins were separated by SDS-PAGE. As shown in Fig. 1C, in comparison to the corona of NPs, the M-NPs yielded a protein pattern consisting of less protein bands with considerably lower intensity. To determine whether M-NPs showed increased resistance to elimination by MPS, we used a macrophage cell line (RAW 264.7) to simulate MPS clearance *in vitro* by evaluating the cellular uptake of NPs and M-NPs. RAW264.7 cells were cultured with Rhodamine B-labeled NPs or M-NPs for 60 min, followed by visualization with confocal microscopy. Compared to the cells treated with NPs, reduced fluorescent signals can be observed in the group treated with M-NPs. Consistent with the confocal microscopy results, the mean fluorescence intensity (MFI) in M-NPs-treated cells also significantly decreased in comparison with NPs treated group, indicating reduced macrophage uptake of LX2 membrane-coated nanoparticles (Fig. 1D). DiR-labeled NPs and M-NPs were further intravenously injected into ICR mice to evaluate the systemic circulation time. At designated time points following the injection, the peripheral blood of mice was collected for fluorescence signal detection. As shown in Fig. 1E, the fluorescence signals in NPs group were nearly undetectable after 30 min, whereas the fluorescence in M-NPs group can be still observed after 2 h of injection, indicating superior blood retention of M-NPs. The non-specific accumulation of both nanoparticles in the liver was also detected by IVIS imaging, which showed that M-NPs had reduced tendency to accumulate in the liver compared with NPs (Fig. 1F).

3.2. Chloroquine treatment showed superior suppression of M-NPs endocytosis in macrophages than tumor cells

Cancer therapy requires cell-specific localization of nanoparticles to improve the therapeutic efficacy and reduce systemic toxicity. To investigate the tumor-specific accumulation of M-NPs, an orthotopic hepatocellular carcinoma (HCC) model was established by intrahepatic injection of Huh7 tumor cells in mice (Fig. 2A). NPs and M-NPs were first labeled with the fluorescent dye Rhodamine B. Subsequently, the distribution of two nanoparticles in different cell types in the liver was determined at 10 min post-injection by measuring the Rhodamine B signal *via* flow cytometry. As shown in Fig. 2B, Kupffer cells showed the highest MFI

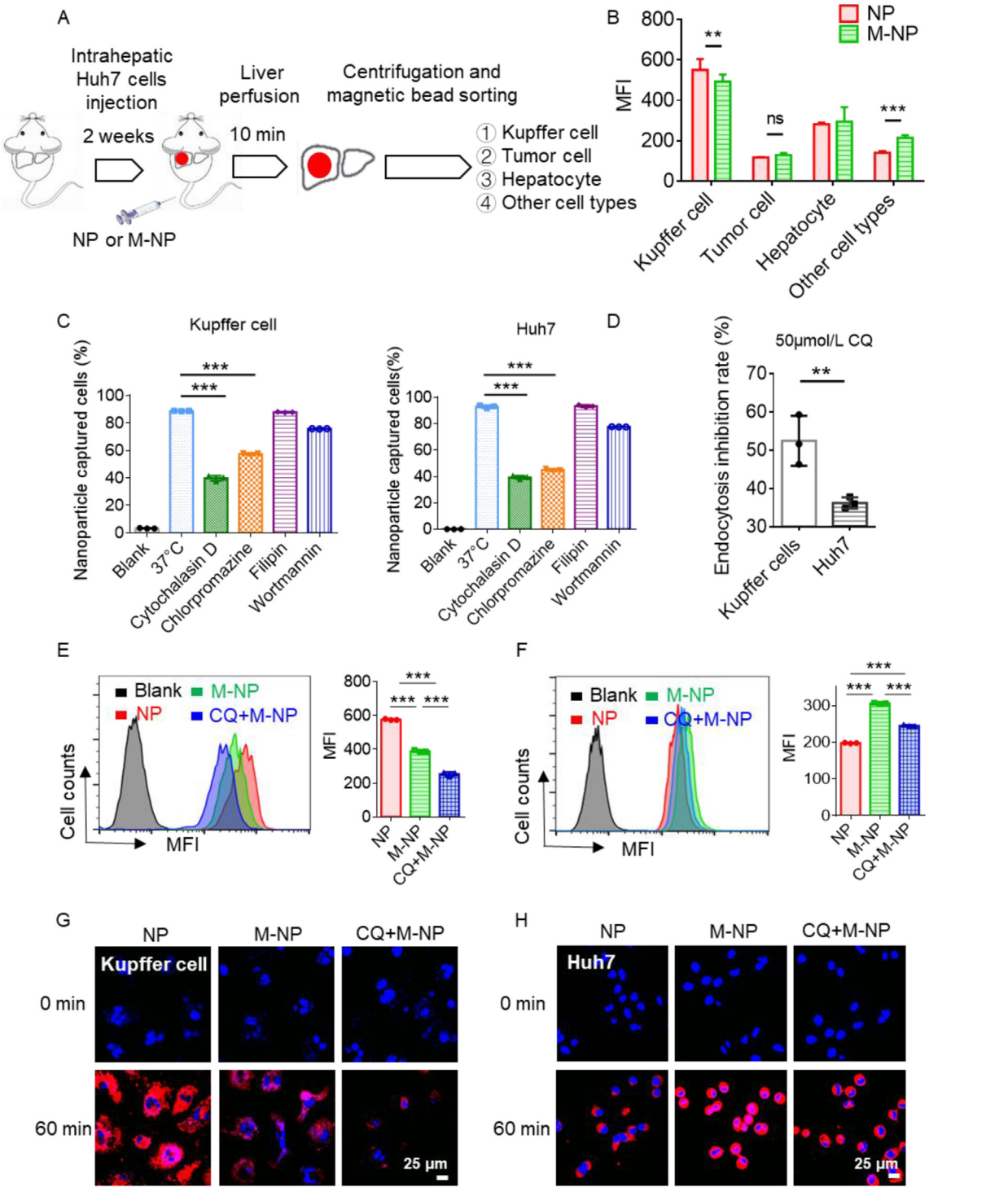

Figure 2 Chloroquine exhibited superior suppression of M-NPs endocytosis in macrophages than tumor cells. (A) Schematic diagram of the establishment of hepatocarcinoma cell orthotropic model and cell sorting. (B) Mean fluorescence intensity (MFI) of each hepatic cell type at 10 min post-injection. ($n = 5$). (C) Effect of endocytosis inhibitors on M-NPs uptake in Kupffer cells and tumor cells. Kupffer cells and Huh7 cells were pretreated with each inhibitor for 0.5 h and then cultured with Rhodamine B loaded M-NPs (Rhodamine B-equivalent dose, 0.13 μg/mL) in 10% serum medium for 2 h at 37 °C followed by flow cytometry detection. A total of 10,000 cells were collected and data are presented as the mean ± SD ($n = 3$). (D) Effect of chloroquine on inhibiting cellular uptake of M-NPs. Kupffer and Huh7 cells treated with 50 μmol/L chloroquine for 2 h at 37 °C were incubated with Rhodamine B-labeled M-NPs for 2 h and the fluorescence intensity in cells was detected by flow cytometry. A total of 10,000 cells were collected and data are presented as the mean ± SD ($n = 3$). Quantitative analysis of the uptake of NPs and M-NPs with or without CQ pretreatment in (E) Kupffer and (F) Huh7 cells by flow cytometry. Cells were incubated with NPs or M-NPs for 1 h. A total of 10,000 cells were collected and data are presented as the mean ± SD ($n = 3$). (G) Confocal microscopy images demonstrating the cell internalization of nanoparticles in Kupffer and (H) Huh7 cells. Cells were incubated with NPs and M-NPs for 1 h. The red fluorescence indicated Rhodamine B-labeled nanoparticles, and cell nuclei were stained in blue with Hochest33342. Scale bar = 25 μm $^*P < 0.05$, $^{**}P < 0.01$, $^{***}P < 0.001$, ns, not significant.

compared with other cell types in both NPs and M-NPs-treated groups. The results give evidence that among all liver cell types Kupffer cells play the most important role in nanomaterial sequestration. Specifically, Kupffer cells in M-NPs group displayed reduced MFI compared with the NPs group (492.4 ± 34.70 *vs*. 550.6 ± 52.83), indicating decreased sequestration of nanoparticles by the MPS. However, tumor cells in NPs and M-NPs groups exhibited weak and almost equal fluorescence signals, which suggests that the LX2 membrane coating strategy was yet insufficient to increase the tumor accumulation of systemically delivered PLGA nanoparticles.

The remained sub-optimal tumor accumulation was possibly due to the insufficient (~10%) inhibition of macrophage entrapment of M-NPs. Therefore, a promising approach to improve the distribution of M-NPs in the tumor was to further decrease macrophage uptake of M-NPs and promote tumor cell endocytosis of the particles. We first hypothesized that Kupffer cells and tumor cells may possess distinct endocytosis pathways for nanoparticle uptake. If so, efforts can be devoted to selectively inhibiting the endocytosis of Kupffer cells without disturbing the nanoparticle uptake of tumor cells. To investigate the endocytosis of Kupffer cells, we isolated Kupffer cells (F4/80+) by using magnetic-activated cell sorting[1] from mouse livers (Supporting Information Fig. S2). The endocytosis pathway study was then performed by using DiR-labeled M-NPs. Well-established small molecule inhibitors were used to suppress specific pathways of particle uptake. As shown in Fig. 2C, filipin (an inhibitor of caveolae-mediated endocytosis) and wortmannin (a micropinocytosis inhibitor) showed marginal effect to inhibit the uptake of M-NPs in both Kupffer cells and Huh7 tumor cells, whereas chlorpromazine (an inhibitor of clathrin-mediated endocytosis) and cytochalasin D (a broad-spectrum inhibitor of actin-dependent uptake) decreased the internalization of M-NPs (~50%) in the two cell lines. These results demonstrated that the engulfment of M-NPs in both Kupffer cells and Huh7 was mainly through clathrin-mediated endocytosis, suggesting that blocking the internalization of nanoparticles in macrophages but not tumor cells by using inhibitors for a specific endocytosis pathway can easily fail. Nevertheless, chloroquine (CQ), an FDA-approved antimalarial drug, has been reported to potently suppress nanoparticle uptake in macrophages without reducing the nanoparticle internalization in non-phagocytic cells, which therefore serves as a promising candidate to improve the tumor accumulation of delivered nanoparticles[37]. Compared to chlorpromazine, CQ was more effective in preventing the uptake of M-NPs in Kupffer cells, suggesting that additional mechanisms beyond suppression of clathrin-mediated internalization may be involved. Tumor cells take up nanoparticles by pinocytosis, including macropinocytosis, clathrin-mediated, caveolin-mediated and clathrin/caveolae-independent endocytosis[52], whereas macrophages uptake nanoparticles not only through pinocytosis, but also *via* phagocytosis[52,53]. As an autophagy inhibitor, CQ prevents lysosome acidification and decreases LC3-associated phagocytosis[54]. Thus, the inhibition of phagocytosis by CQ could result in the superior uptake reduction of nanoparticles in macrophages. Prior to assessing the specificity of CQ in inhibiting nanoparticle internalization in Kupffer and tumor cells, cell viability assays were performed to determine the toxicity of this agent (Supporting Information Fig. S3). Finally, CQ at a non-toxic concentration (50 μmol/L) was used for cell treatment to study its endocytosis inhibition in different cell lines. Consistent with previous investigation, CQ was more effective in preventing nanoparticle uptake in macrophages (Kupffer and RAW264.7) than tumor cells (Huh7 and CT26) (Fig. 2D and Supporting Information Fig. S4).

The impacts of cell membrane coating and CQ pretreatment on nanoparticle uptake *in vitro* were then investigated by flow cytometry in Kupffer cells and Huh7. Results showed that Kupffer cells treated with M-NPs presented reduced fluorescence intensity of Rhodamine B compared to NPs treated cells, indicating suppressed uptake of nanoparticles (Fig. 2E). In contrast, M-NPs-treated Huh7 cells exhibited increased nanoparticle uptake in comparison with NPs treated cells (Fig. 2F). Notably, CQ pretreatment decreased M-NPs internalization in both cell lines. However, Huh7 cells pretreated with CQ still showed improved nanoparticle uptake when treated with M-NPs in comparison with NPs treated cells. The confocal microscopy detection further confirmed these results (Fig. 2G and H), which suggests that the combination of LX2 membrane coating and CQ treatment may provide a feasible approach for improving the tumor targeting of systemic delivered nanoparticles.

3.3. *Chloroquine treatment improved the biodistribution of M-NPs and increased their internalization in tumor cells*

We next investigated the effect of CQ treatment on nanoparticle biodistribution. For this study, 12 mice were randomly separated into 3 groups with 4 mice for each group. Two groups were administered intravenously with DiR-labeled NPs and M-NPs, respectively, whereas the mice in the third group were treated with CQ (40 mg/kg/day) for 3 days *via* intraperitoneal injection, followed by the administration of DiR-loaded M-NPs. After 6 h of injection, major organs and blood were collected and homogenized to evaluate the distribution of nanoparticles by measuring the fluorescence signals (Supporting Information Fig. S5). As the fluorescence in the liver of M-NPs-treated group decreased compared with NPs treated mice, a corresponding increase in signal was observed in the blood. Notably, mice with CQ treatment showed the least fluorescence intensity in the liver and the highest signal in the blood (Fig. 3B). These results indicated that the combination of LX2 membrane coating and CQ-based macrophage preconditioning was efficient to decrease the sequestration of nanoparticles by the MPS for prolonged blood circulation.

Subsequently, we investigated the effect of the combination strategy on tumor accumulation of nanoparticles by using an orthotopic hepatocellular carcinoma (HCC) model. We first established the HCC tumor by intrahepatic injection of Huh7 cells stably expressing luciferase, followed by the treatment of CQ for continuous 3 days and the administration of DiR-labeled M-NPs (Fig. 3C). As shown in Fig. 3D, tumor sites (circled with white lines) were identified by bioluminescence, and the fluorescence intensity in the tumor was further quantified with ImageJ. It is worth noting that compared with NPs treated mice, M-NPs-treated mice (with or without CQ pretreatment) showed decreased nanoparticle uptake in the tumor area (Fig. 3E). Based on the tumor cell targeting potential of LX2 membrane coating, this result could be attributed to the reduced nanoparticle internalization in tumor-associated macrophages, which can constitute up to 50% of the cell population in some solid tumors[55–57]. As such, detailed nanoparticle distribution was determined in different liver cell types *in vivo*, including tumor cells, hepatocytes, Kupffer cells and other cell types. We first determined the portion of each cell type among the entire liver cell population (Supporting Inforamtion Fig. S6A). Cell sorting results indicated the tumor

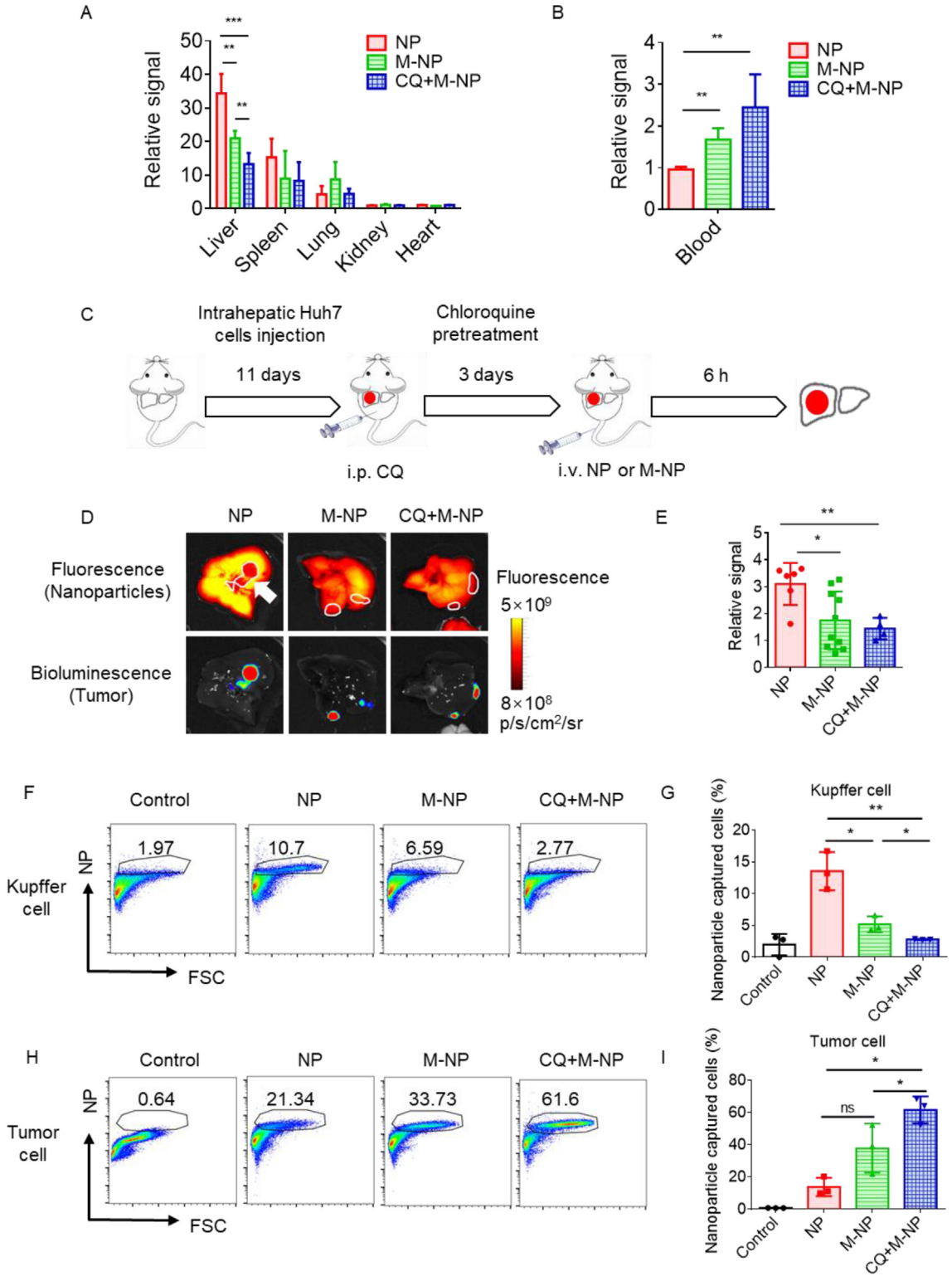

Figure 3 Chloroquine treatment improved the biodistribution of M-NPs and increased their internalization in tumor cells. (A) Quantification of the distribution of NPs and M-NPs with or without CQ pretreatment in major organs and (B) blood by measuring the fluorescence intensity of homogenized tissues at 6 h post-injection. (C) Schematic diagram of CQ treatment and nanoparticle administration in the hepatocarcinoma cell orthotropic tumor bearing mice. (D) IVIS fluorescence and bioluminescence images of livers collected at 6 h post-injection of nanoparticles. Tumor sites were marked with white lines based on bioluminescence detection. (E) Quantification of MFI in the tumor sites. (F) Representative flow plots and (G) quantitative analysis of nanoparticle uptake in Kupffer cells of livers that were collected from tumor bearing mice at 6 h post-injection of nanoparticles. (H) Representative flow plots and (I) quantitative analysis of nanoparticle uptake in tumor cells of livers that were collected from tumor bearing mice at 6 h post-injection of nanoparticles. $^{*}P < 0.05$, $^{**}P < 0.01$, $^{***}P < 0.001$, ns, not significant.

bearing liver tissues contain 44.62±3.27% of hepatocytes, 7.06±1.14% tumor cells, 12.51±0.75% of Kupffer cells and 35.80±2.02% of other cell types. We next analyzed the percentage of Rhodamine B-positive cells in Kupffer cells and tumor cells after the injection of different nanoparticles. As shown in Fig. 3F and G, M-NPs and CQ + M-NPs treatment significantly reduced the nanoparticle uptake in Kupffer cells. In contrast, CQ + M-NPs group showed dramatically enhanced tumor cell uptake of nanoparticles compared with the NPs group (Fig. 3H and I). These results demonstrated that alteration of nanoparticles physicochemical properties cannot single-handedly solve the delivery obstacles. The combination of nanoparticle design and MPS modulation could be an effective strategy for improved site-specific drug delivery.

3.4. TRAIL-expressing cell membrane-coated CQ-loaded PLGA nanoparticles (TM-CQ/NPs) selectively induced tumor cell apoptosis

For therapeutic purpose, we developed a flexible approach to express TRAIL onto the cell membrane to selectively induce tumor cell apoptosis. We first established the LX2-TRAIL-ZSGREEN cell line, with TRAIL-ZSGREEN fusion protein expressed on the membrane of LX2 cells. To confirm the successful establishment of the cell line, we used confocal microscopy imaging and showed that the engineered cells were positive for ZSGREEN expression (Fig. 4A). Western blotting results demonstrated that cell membrane isolated from LX2-TRAIL-ZSGREEN cells but not normal LX2 cells expresses TRAIL, which confirmed the anchoring of TRAIL on the membrane of engineered LX2 cells (Fig. 4B). In addition, as shown in Supporting Inforamtion Fig. S7, we found the stable expression of TRAIL-ZSGREEN did not affect the transmembrane proteins CD47 and N-cadherin. N-cadherin is involved in the heterotypic adhesion between fibroblasts and tumor cells[33], which plays an important role in tumor-site targeting. Meanwhile, the display of "don't eat me" signal CD47 on both LX2 and LX2-TRAIL-ZSGREEN cell membrane could reduce macrophage uptake[58]. In addition, fibroblast membrane wrapping reduced the protein corona on nanoparticles (Fig. 1C) and may result in decreased macrophage uptake[59]. M-NPs and TM-NPs presented comparable blood circulation. Thus, expressing TRAIL-ZSGREEN on LX2 cell membrane didn't affect the blood circulation of M-NPs (Supporting Information Fig. S8).

To fabricate TM-CQ/NPs, CQ/NPs were prepared by single emulsion followed by the coating of TRAIL-expressing cell membranes *via* extrusion. CQ/NPs exhibited drug loading efficiency about 8.5%, along with 76.3% drug encapsulation efficiency. Representative TEM images of TM-CQ/NPs showed a typical core-shell structure with an average diameter of around 200 nm (Fig. 4C). We also measured the hydrodynamic diameter and polydispersity of CQ/NPs and TM-CQ/NPs using DLS to verify that they are monodisperse and stable. As shown in Fig. 4D, the hydrated size of TM-CQ/NPs was approximately 221.3±13.1 nm. The coated nanoparticles exhibited an increase in diameter of 17.2 nm compared to CQ/NPs. As shown in Fig. 4E, uncoated CQ/NPs possessed similar surface charge around −3 mV in different buffers. However, the coated nanoparticles had a zeta potential of −23.5 mV in deionized water, while −8.4, −9.3 and −8.6 mV in PBS, NaCl and Hanks buffer, respectively. The changes in surface charge states indicated that CQ/NPs were successfully coated with LX2 membranes. These experimental results suggested that CQ/NPs are superior carriers with good drug encapsulation, and desirable particle size.

CQ released slowly from CQ/NPs in PBS (pH7.4 and 6.8) containing 1% Tween. Besides, the release rate of CQ was accelerated in acid buffer (pH 4.5) due to the acid-triggered cleavage of ester bonds of PLGA (Fig. 4F). For the blood clearance study, the CQ plasma concentrations at different time intervals after i.v. administration of CQ/NPs or TM-CQ/NPs were measured using HPLC. Compared to CQ/NPs, TM-CQ/NPs remarkably prolonged the circulation of CQ in blood stream (Fig. 4G). In addition, the biodistributions of CQ in CQ/NPs and TM-CQ/NPs were determined in ICR mice after a single i.v. injection of CQ/NPs or TM-CQ/NPs at an equivalent CQ dose of 40 mg/kg (Fig. 4H). As expected, membrane coating decreased the CQ liver concentration from 31.1 ± 4.1 to 9.1 ± 0.9 μg/g but increased the blood concentration from 3.4 ± 0.1 to 7.3 ± 1.42 μg/g.

To validate the tumor-selective apoptotic effect of TRAIL on TM-CQ/NPs, we determined the cytotoxicity of M-NPs, TM-NPs, CQ/NPs, M-CQ/NPs and TM-CQ/NPs in CT26, Huh7 and RAW264.7 cell lines by crystal violet staining. Of note, treatment of tumor cells with TM-NPs and TM-CQ/NPs significantly decreased the cell viability, whereas CQ/NPs and M-CQ/NPs showed marginal effect to inhibit tumor cell growth. More importantly, TM-CQ/NPs exhibited enhanced efficacy to inhibit tumor cell growth compared to TM-NPs, suggesting that incorporated CQ synergized with TRAIL to induce tumor cell apoptosis. This superior therapeutic efficacy of TM-CQ/NPs can attribute to inhibited protective autophagy[60] and upregulation of death receptors by CQ[61], resulting in increased sensitivity of tumor cells to TRAIL. As expected, all treatments had no obvious cytotoxicity on the non-transformed RAW264.7 cells (Fig. 4I). Consistent with the results of cytotoxicity assay, treatment with TM-CQ/NPs caused increased processing of poly-ADP-ribose polymerase (PARP) cleavage in CT26 and Huh7 cells compared to TM-NPs treatment, and other treatments showed no obvious PARP cleavage (Fig. 4J). These results demonstrated that TM-CQ/NPs were efficient in selectively inducing tumor cell apoptosis.

3.5. TM-CQ/NPs suppressed tumor growth in multiple tumor models

The HCC tumor model in nude mice was first used to evaluate the antitumor effect of TM-CQ/NPs. Huh7 cells stably expressing luciferase were employed to establish the model for non-invasive detection of tumor growth and metastasis using an IVIS imaging system. The treatment schedule is presented in Fig. 5A. After 14 days of tumor cell inoculation, mice were randomly grouped, following treatments with PBS, TM-NPs, CQ/NPs, or TM-CQ/NPs as scheduled. The plasma half-life of CQ in ICR mice was 46.6 h[62]. Four injections were given in the antitumor study. After the first injection, the CQ released from nanoparticles could maintain effective concentration *in vivo* for the upcoming treatments. In addition, our previous study indicated that Nano-CQ showed longer blood circulation and enhanced tumor accumulation than free CQ[63]. Tumor growth was monitored by IVIS imaging (Fig. 5B). While TM-NPs and CQ/NPs showed limited antitumor efficacy, TM-CQ/NPs significantly inhibited the tumor growth (Fig. 5C). In addition, the overall survival analysis indicated that the TM-CQ/NPs treatment improved the median

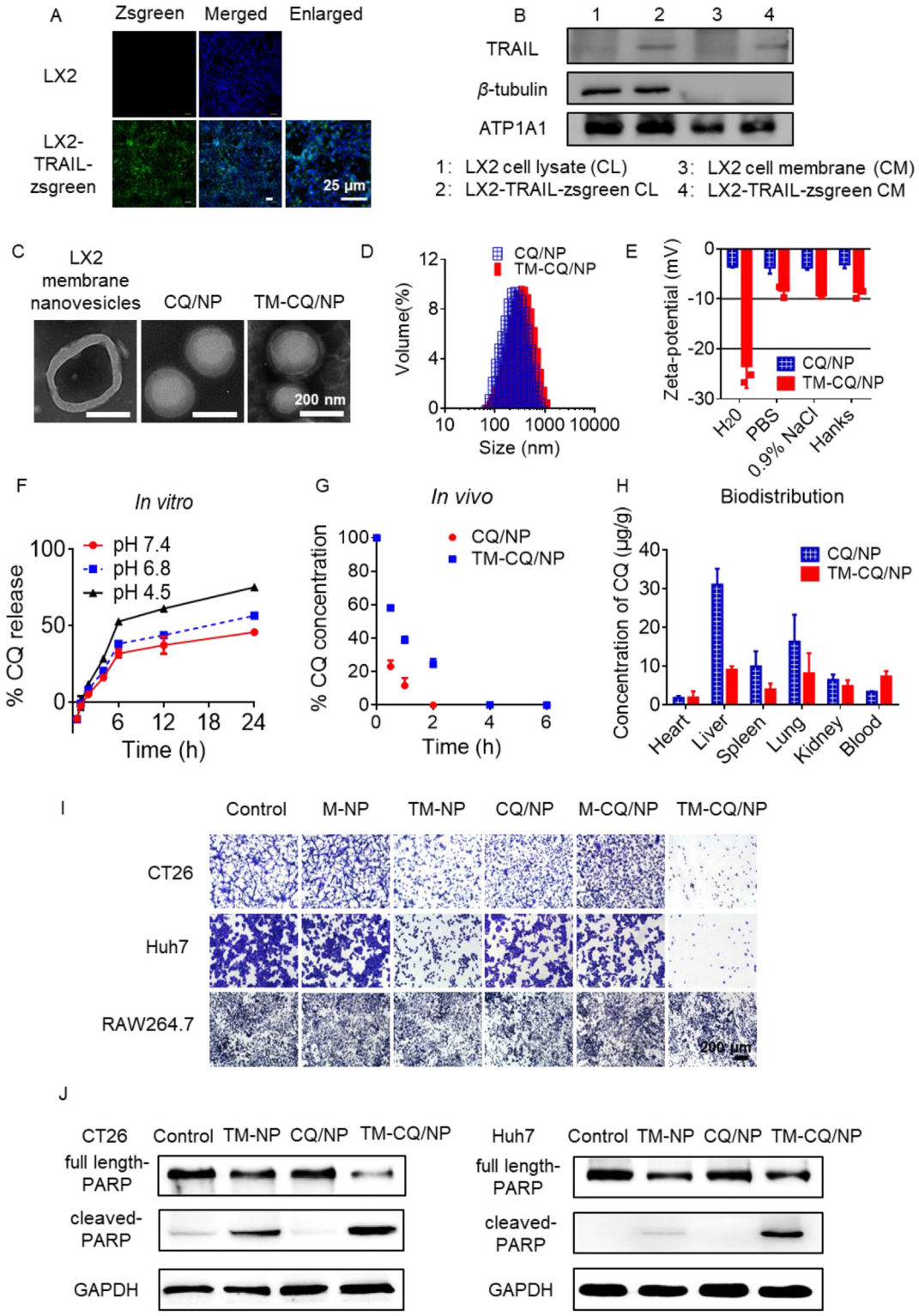

Figure 4 TM-CQ/NPs selectively induced tumor cell apoptosis *in vitro*. (A) Establishment of LX2 cell line stably expressing TRAIL-zsgreen fusion protein on the cell membrane. Cell nuclei (blue) were stained with Hochest33342. Scale bar = 25 μm. (B) Detection of TRAIL in whole cell lysate and cell membrane of LX2 or LX2-TRAIL-zsgreen cells by Western blot. β-Tubulin and ATP1A1 were used as the loading controls. (C) TEM images of TRAIL-expressing-LX2 membrane (TM), CQ loaded PLGA nanoparticles (CQ/NPs) and TM coated CQ/NPs (TM-CQ/NPs). All samples were stained with phosphotungstic acid. Scale bar = 200 nm. (D) DLS measured diameter of CQ/NPs and TM-CQ/NPs in PBS buffer. (E) Zeta potential measurements of CQ/NPs and TM-CQ/NPs in deionized water, PBS, 0.9% NaCl and Hanks buffer (pH7.4). (F) Determination of release behavior of CQ in CQ/NPs ($n = 3$). (G) Quantitative analysis of blood circulation of nanoparticles by measuring the CQ concentration in whole blood ($n = 3$). (H) CQ concentration in main organs of ICR mice at 6 h post-intravenous administration of CQ/NPs and

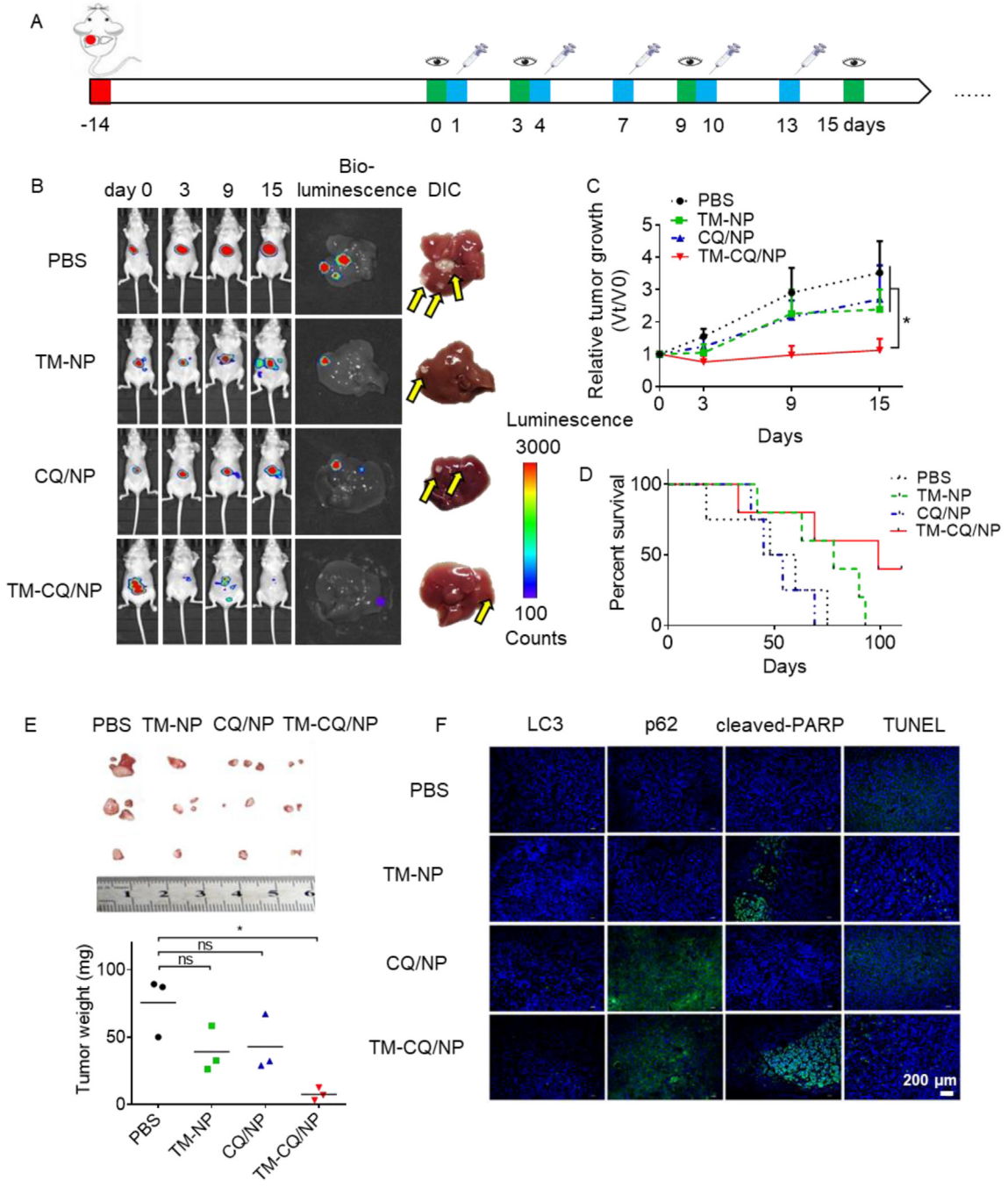

Figure 5 TM-CQ/NPs inhibited the tumor growth in orthotropic HCC tumor model. (A) Schematic illustration of intravenous dosing schedule of different formulations (PBS, TM-NPs, CQ/NPs and TM-CQ/NPs) in Huh7 tumor-bearing nude mice. (B) Representative bioluminescence images of Huh7 tumor-bearing mice during the treatment. At the end of the treatment livers from tumor bearing mice were collected and bright field images were acquired with tumors marked with yellow arrows. (C) Tumor growth monitored by IVIS imaging after different treatments. (D) Kaplan-Meier survival curves of nude mice after treatments ($n = 4$ or 5). (E) Images of dissected tumors and the average tumor weight at the end of different treatments ($n = 3$). (F) Immunofluorescence staining (LC3, p62, and cleaved-PARP) and TUNEL assay of tumor tissues from mice with different treatments. $^*P < 0.05$, ns, not significant.

survival (99 days) compared with PBS group (54 days) (Fig. 5D). Tumors dissected from tumor bearing mice in TM-CQ/NPs group also exhibited the lowest tumor weight compared to other treatments, which confirmed its prominent therapeutic efficacy (Fig. 5E). Immunofluorescence staining was performed to determine the *in vivo* anticancer mechanism. Elevated expression of

TM-CQ/NPs ($n = 5$). (I) Crystal violet staining of CT26, Huh7 and RAW264.7 cells treated with different nanoparticles (M-NPs, TM-NPs, CQ/NPs, M-CQ/NPs and TM-CQ/NPs) for 24h. Scale bar = 200 μm. (J) Analysis of full-length and cleaved PARP in CT26 and Huh7 cells after 24 h treatment with different nanoparticles (TM-NPs, CQ/NPs and TM-CQ/NPs). GAPDH was used as the loading control.

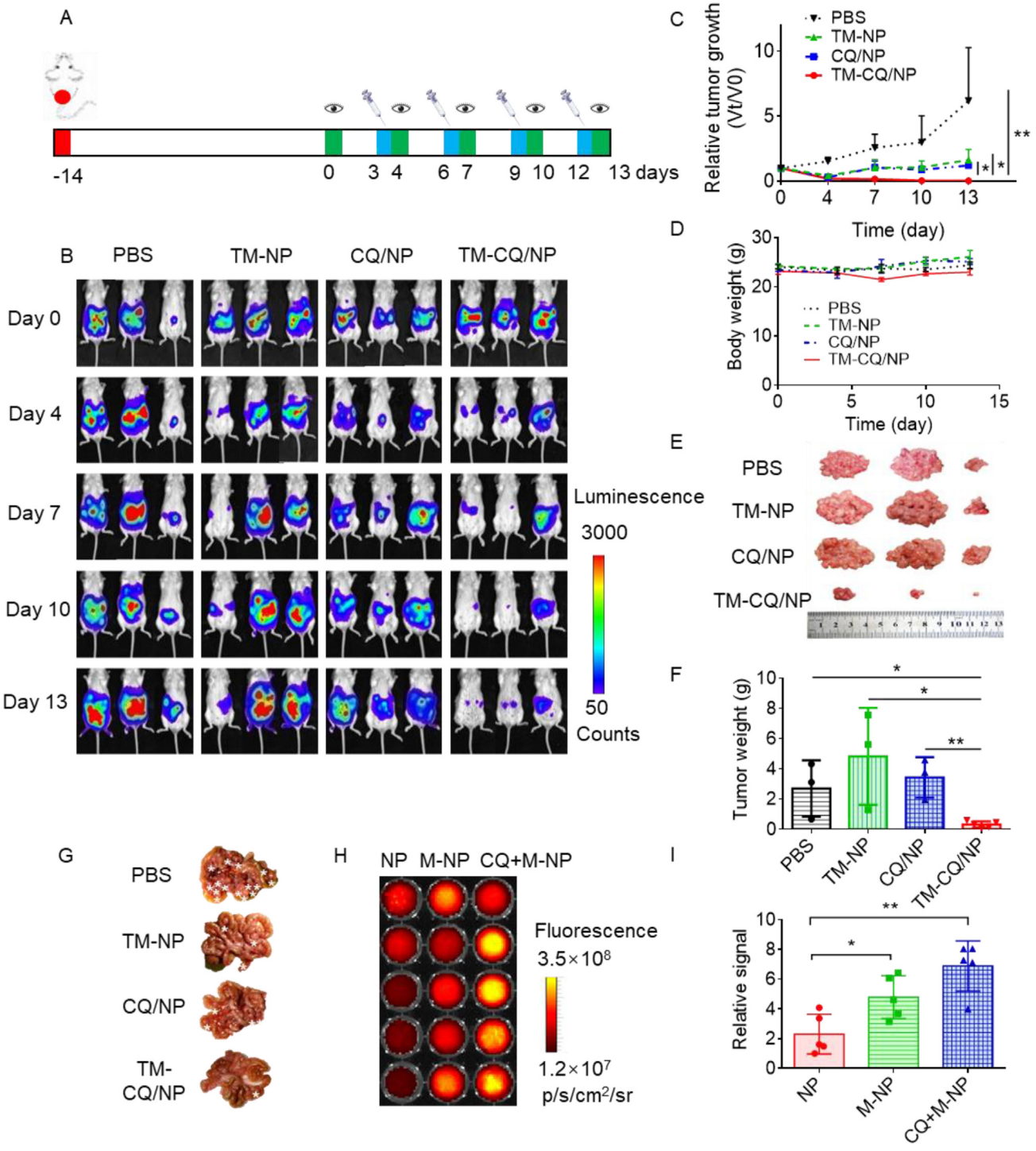

Figure 6 TM-CQ/NPs suppressed the tumor growth in intraperitoneal tumor model. (A) Schematic illustration of dosing and IVIS imaging schedules for different treatments. (B) Bioluminescence images of CT26 tumor-bearing mice during the treatment. (C) Tumor growth monitored by IVIS imaging after different treatments. (D) Body weight curves of tumor-bearing mice ($n = 3$). (E) Dissected intraperitoneal tumor nodules after sacrifice of mice. (F) The average tumor weight at the end of the treatment ($n = 3$ or 5). (G) Representative images of tumor nodules distribution in mesentery. The asterisks represent tumor nodules. (H) Detection and (I) quantitative analysis of the tumor accumulation of NPs and M-NPs with or without CQ pretreatment in the CT26 intraperitoneal tumor model ($n = 5$). Fluorescently labeled nanoparticles were injected intravenously into the tumor-bearing mice and tumors were collected, homogenized, and quantified for fluorescence 24 h post injection. $^{*}P < 0.05$, $^{**}P < 0.01$.

LC3B and p62 in tumors from CQ/NPs and TM-CQ/NPs treated mice was observed, indicating effective suppression of autophagy. Importantly, tumors from TM-CQ/NPs treated mice displayed increased cleaved-PARP compared with those in TM-NPs-treated mice, which was consistent with the *in vitro* findings. TUNEL (a biomarker for apoptosis) assay confirmed that TM-CQ/NPs

elicited the strongest apoptotic effect compared with other treatments (Fig. 5F).

An intraperitoneal tumor model was further employed to evaluate the antitumor effects of TM-CQ/NPs. The intraperitoneal tumor model was generated by i.p. inoculation with CT26 cells expressing luciferase (CT26-luci). Mice received four i.p. injections of PBS, TM-NPs, CQ/NPs or TM-CQ/NPs as scheduled (Fig. 6A). Tumor burden was recorded using bioluminescence imaging (Fig. 6B). The tumor growth in TM-CQ/NPs treated mice was significantly slower than that of the PBS, TM-NPs or CQ/NPs group (Fig. 6C) without obvious body weight changes (Fig. 6D). As shown in Fig. 6E and F, the average tumor weights in the TM-CQ/NPs group (0.32 ± 0.21 g) was much lower than those in the PBS (2.70 ± 1.86 g), TM-NPs (4.82 ± 3.21 g), and CQ/NPs (3.43 ± 1.34 g)-treated groups. TM-CQ/NPs treatment exhibited less scattered tumor nodules on the mesentery compared to other treatments (Fig. 6G).

Importantly, the effect of CQ pretreatment on (DiR-labeled) M-NPs accumulation in tumors was evaluated in mice bearing CT26-luci intraperitoneal tumors. Notably, compared with NPs treated group, CQ + M-NPs group showed improved tumor accumulation of nanoparticles (Fig. 6H and I), which may account for the significant effects on tumor growth inhibition of TM-CQ/NPs.

3.6. TM-CQ/NPs exhibited no obvious toxicity

The potential toxicity of nanoparticles remains a major concern for clinical translation. Here, H&E staining was performed to evaluate the histological abnormality of major organs including heart, liver, spleen, lung, and kidney after different treatments. TM-CQ/NPs group showed no obvious histological abnormalities, demonstrating that TM-CQ/NPs did not induce drastic side effects (Supporting Inforamtion Fig. S9A). Considering the accumulation of nanoparticles in the liver and the potent hepatotoxicity of TRAIL, hepatorenal functions and blood routine analysis in ICR mice were performed after various treatments. The results showed that the alanine aminotransferase (ALT), serum aspartate aminotransferase (AST), and blood urea nitrogen (BUN) remained constant for all treatment groups (Fig. S9B). Besides, no abnormal changes in the complete blood count were observed in each group (Fig. S9C), indicating that no severe toxicity was induced following these treatments.

4. Conclusions

In this study, we not only developed a strategy to overcome the MPS barrier for tumor-targeted delivery *via* combining biomimetic coating with macrophage modulation, but also reported an easily-produced method to prepare an apoptosis inducing nanosystem specifically targeting tumor cells. The key factors involved in the nanosystem design include: 1) Membrane of fibroblast cells was firstly used as a coating material to evade macrophage uptake of nanoparticles, but to facilitate the endocytosis of nanoparticles in tumor cells. 2) The tumor specific apoptosis-inducer TRAIL was expressed on the coated membrane, endowing the membrane with selective antitumor capability. 3) The encapsulated CQ remodeled macrophages to further reduce the uptake of upcoming nanoparticles, while CQ synergized with TRAIL to trigger vigorous antitumor effect.

Acknowledgments

This work was supported by the National Natural Science Foundation of China (Nos. 32101128, 21975218, and 51773176), the National Key Research and Development Program of China (2019YFA0802202), and the 111 Project (B13026, China). We thank Jiafeng Zhong at College of Chemical and Biological Engineering of Zhejiang University for his constant supply of LX2 cells.

Author contributions

Xiangrui Liu and Tianhua Zhou conceptualized original idea and designed the experiments; Zimo Liu, Xuefei Zhou and Qi Li performed experiments; Xuefei Zhou, Zimo Liu, and Xiangrui Liu wrote the manuscript and were involved in data analysis; Youqing Shen provided experimental support.

Conflicts of interest

The authors declare no conflicts of interest.

Appendix A. Supporting information

Supporting data to this article can be found online at https://doi.org/10.1016/j.apsb.2022.05.010.

References

1. Mitchell MJ, Billingsley MM, Haley RM, Wechsler ME, Peppas NA, Langer R. Engineering precision nanoparticles for drug delivery. *Nat Rev Drug Discov* 2021;**20**:101−24.
2. Riley RS, June CH, Langer R, Mitchell MJ. Delivery technologies for cancer immunotherapy. *Nat Rev Drug Discov* 2019;**18**:175−96.
3. Zhang W, Wang F, Hu C, Zhou Y, Gao H, Hu J. The progress and perspective of nanoparticle-enabled tumor metastasis treatment. *Acta Pharm Sin B* 2020;**10**:2037−53.
4. Anselmo AC, Mitragotri S. Nanoparticles in the clinic: an update. *Bioeng Transl Med* 2019;**4**:e10143.
5. Marques MRC, Choo Q, Ashtikar M, Rocha TC, Bremer-Hoffmann S, Wacker MG. Nanomedicines—tiny particles and big challenges. *Adv Drug Deliv Rev* 2019;**151-152**:23−43.
6. Wilhelm S, Tavares AJ, Dai Q, Ohta S, Audet J, Dvorak HF, et al. Analysis of nanoparticle delivery to tumours. *Nat Rev Mater* 2016;**1**:16014.
7. Gustafson HH, Holt-Casper D, Grainger DW, Ghandehari H. Nanoparticle uptake: the phagocyte problem. *Nano Today* 2015;**10**:487−510.
8. Gordon S. Phagocytosis: an immunobiologic process. *Immunity* 2016;**44**:463−75.
9. Blanco E, Shen H, Ferrari M. Principles of nanoparticle design for overcoming biological barriers to drug delivery. *Nat Biotechnol* 2015;**33**:941−51.
10. Zhou H, Fan Z, Li PY, Deng J, Arhontoulis DC, Li CY, et al. Dense and dynamic polyethylene glycol shells cloak nanoparticles from uptake by liver endothelial cells for long blood circulation. *ACS Nano* 2018;**12**:10130−41.
11. Pasut G, Veronese FM. State of the art in PEGylation: the great versatility achieved after forty years of research. *J Contr Release* 2012;**161**:461−72.
12. Mishra P, Nayak B, Dey RK. PEGylation in anti-cancer therapy: an overview. *Asian J Pharm Sci* 2016;**11**:337−48.

13. Schellekens H, Hennink WE, Brinks V. The Immunogenicity of polyethylene glycol: facts and fiction. *Pharm Res (N Y)* 2013;**30**:1729−34.
14. Hu CMJ, Zhang L, Aryal S, Cheung C, Fang RH, Zhang LF. Erythrocyte membrane-camouflaged polymeric nanoparticles as a biomimetic delivery platform. *Proc Natl Acad Sci U S A* 2011;**108**:10980−5.
15. Zhou JR, Kroll AV, Holay M, Fang RH, Zhang LF. Biomimetic nanotechnology toward personalized vaccines. *Adv Mater* 2020;**32**:1901255.
16. Liu X, Zhong X, Li C. Challenges in cell membrane-camouflaged drug delivery systems: development strategies and future prospects. *Chin Chem Lett* 2021;**32**:2347−58.
17. Belhadj Z, He B, Deng H, Song S, Zhang H, Wang X, et al. A combined "eat me/don't eat me" strategy based on extracellular vesicles for anticancer nanomedicine. *J Extracell Vesicles* 2020;**9**:1806444.
18. Chen Q, Wang C, Zhang XD, Chen GJ, Hu QY, Li HJ, et al. *In situ* sprayed bioresponsive immunotherapeutic gel for post-surgical cancer treatment. *Nat Nanotechnol* 2019;**14**:89−97.
19. Zhu JY, Zheng DW, Zhang MK, Yu WY, Qiu WX, Hu JJ, et al. Preferential cancer cell self-recognition and tumor self-targeting by coating nanoparticles with homotypic cancer cell membranes. *Nano Lett* 2016;**16**:5895−901.
20. Li J, Zhen X, Lyu Y, Jiang Y, Huang J, Pu K. Cell membrane coated semiconducting polymer nanoparticles for enhanced multimodal cancer phototheranostics. *ACS Nano* 2018;**12**:8520−30.
21. Liu Y, Luo J, Chen X, Liu W, Chen T. Cell membrane coating technology: a promising strategy for biomedical applications. *Nano-Micro Lett* 2019;**11**:100.
22. Dehaini D, Wei XL, Fang RH, Masson S, Angsantikul P, Luk BT, et al. Erythrocyte-platelet hybrid membrane coating for enhanced nanoparticle functionalization. *Adv Mater* 2017;**29**:1606209.
23. Ben-Akiva E, Meyer RA, Yu H, Smith JT, Pardoll DM, Green JJ. Biomimetic anisotropic polymeric nanoparticles coated with red blood cell membranes for enhanced circulation and toxin removal. *Sci Adv* 2020;**6**:eaay9035.
24. von Karstedt S, Montinaro A, Walczak H. Exploring the TRAILs less travelled: TRAIL in cancer biology and therapy. *Nat Rev Cancer* 2017;**17**:352−66.
25. Pitti RM, Marsters SA, Ruppert S, Donahue CJ, Moore A, Ashkenazi A. Induction of apoptosis by Apo-2 ligand, a new member of the tumor necrosis factor cytokine family. *J Biol Chem* 1996;**271**:12687−90.
26. Croft M, Benedict CA, Ware CE. Clinical targeting of the TNF and TNFR superfamilies. *Nat Rev Drug Discov* 2013;**12**:147−68.
27. Naoum GE, Buchsbaum DJ, Tawadros F, Farooqi A, Arafat WO. Journey of TRAIL from bench to bedside and its potential role in immuno-oncology. *Oncol Rev* 2017;**11**:26−42.
28. Gores GJ, Kaufmann SH. Is TRAIL hepatotoxic?. *Hepatology* 2001;**34**:3−6.
29. Jiang HP, Wang SJ, Zhou XF, Wang LY, Ye LD, Zhou ZX, et al. New path to treating pancreatic cancer: TRAIL gene delivery targeting the fibroblast-enriched tumor microenvironment. *J Contr Release* 2018;**286**:254−63.
30. De Miguel D, Gallego-Lleyda A, Ayuso JM, Pejenaute-Ochoa D, Jarauta V, Marzo I, et al. High-order TRAIL oligomer formation in TRAIL-coated lipid nanoparticles enhances DR5 cross-linking and increases antitumour effect against colon cancer. *Cancer Lett* 2016;**383**:250−60.
31. Nair PM, Flores H, Gogineni A, Marsters S, Lawrence DA, Kelley RF, et al. Enhancing the antitumor efficacy of a cell-surface death ligand by covalent membrane display. *Proc Natl Acad Sci U S A* 2015;**112**:5679−84.
32. De Miguel D, Basanez G, Sanchez D, Malo PG, Marzo I, Larrad L, et al. Liposomes decorated with Apo2L/TRAIL overcome chemoresistance of human hematologic tumor cells. *Mol Pharm* 2013;**10**:893−904.
33. Labernadie A, Kato T, Brugues A, Serra-Picamal X, Derzsi S, Arwert E, et al. A mechanically active heterotypic E-cadherin/N-cadherin adhesion enables fibroblasts to drive cancer cell invasion. *Nat Cell Biol* 2017;**19**:224−37.
34. Chen YL, Abraham DJ, Xu SW, Pearson JD, Black CM, Lyons KM, et al. CCN2 (connective tissue growth factor) promotes fibroblast adhesion to fibronectin. *Mol Biol Cell* 2004;**15**:5635−46.
35. Molavi F, Barzegar-Jalali M, Hamishehkar H. Polyester based polymeric nano and microparticles for pharmaceutical purposes: a review on formulation approaches. *J Contr Release* 2020;**320**:265−82.
36. Tavares AJ, Poon W, Zhang YN, Dai Q, Besla R, Ding D, et al. Effect of removing Kupffer cells on nanoparticle tumor delivery. *Proc Natl Acad Sci U S A* 2017;**114**:E10871−80.
37. Wolfram J, Nizzero S, Liu H, Li F, Zhang G, Li Z, et al. A chloroquine-induced macrophage-preconditioning strategy for improved nanodelivery. *Sci Rep* 2017;**7**:13738.
38. Hu TY, Frieman M, Wolfram J. Insights from nanomedicine into chloroquine efficacy against COVID-19. *Nat Nanotechnol* 2020;**15**:247−9.
39. Zhang XD, Dong YC, Zeng XW, Liang X, Li XM, Tao W, et al. The effect of autophagy inhibitors on drug delivery using biodegradable polymer nanoparticles in cancer treatment. *Biomaterials* 2014;**35**:1932−43.
40. Zhang XD, Zeng XW, Liang X, Yang Y, Li XM, Chen HB, et al. The chemotherapeutic potential of PEG-*b*-PLGA copolymer micelles that combine chloroquine as autophagy inhibitor and docetaxel as an anticancer drug. *Biomaterials* 2014;**35**:9144−54.
41. Sun JH, Ye C, Bai EH, Zhang LL, Huo SJ, Yu HH, et al. Co-delivery nanoparticles of doxorubicin and chloroquine for improving the anticancer effect *in vitro*. *Nanotechnology* 2019;**30**:085101.
42. Hoshyar N, Gray S, Han HB, Bao G. The effect of nanoparticle size on *in vivo* pharmacokinetics and cellular interaction. *Nanomedicine* 2016;**11**:673−92.
43. Walkey CD, Olsen JB, Guo H, Emili A, Chan WCW. Nanoparticle size and surface chemistry determine serum protein adsorption and macrophage uptake. *J Am Chem Soc* 2012;**134**:2139−47.
44. Jiang W, Kim BYS, Rutka JT, Chan WCW. Nanoparticle-mediated cellular response is size-dependent. *Nat Nanotechnol* 2008;**3**:145−50.
45. Chithrani BD, Chan WCW. Elucidating the mechanism of cellular uptake and removal of protein-coated gold nanoparticles of different sizes and shapes. *Nano Lett* 2007;**7**:1542−50.
46. Kulkarni SA, Feng S-S. Effects of particle size and surface modification on cellular uptake and biodistribution of polymeric nanoparticles for drug delivery. *Pharm Res (N Y)* 2013;**30**:2512−22.
47. Abdelghany S, Parumasivam T, Pang A, Roediger B, Tang P, Jahn K, et al. Alginate modified-PLGA nanoparticles entrapping amikacin and moxifloxacin as a novel host-directed therapy for multidrug-resistant tuberculosis. *J Drug Deliv Sci Technol* 2019;**52**:642−51.
48. Chen W, Palazzo A, Hennink WE, Kok RJ. Effect of particle size on drug loading and release kinetics of gefitinib-loaded PLGA microspheres. *Mol Pharm* 2017;**14**:459−67.
49. Zhao ZM, Ukidve A, Krishnan V, Mitragotri S. Effect of physicochemical and surface properties on *in vivo* fate of drug nanocarriers. *Adv Drug Deliv Rev* 2019;**143**:3−21.
50. Fang RH, Kroll AV, Gao WW, Zhang LF. Cell membrane coating nanotechnology. *Adv Mater* 2018;**30**:34.
51. Sherman MH, Yu RT, Engle DD, Ding N, Atkins AR, Tiriac H, et al. Vitamin D receptor-mediated stromal reprogramming suppresses pancreatitis and enhances pancreatic cancer therapy. *Cell* 2014;**159**:80−93.
52. de Almeida MS, Susnik E, Drasler B, Taladriz-Blanco P, Petri-Fink A, Rothen-Rutishauser B. Understanding nanoparticle endocytosis to improve targeting strategies in nanomedicine. *Chem Soc Rev* 2021;**50**:5397−434.
53. Chen SQ, Lai SWT, Brown CE, Feng MY. Harnessing and enhancing macrophage phagocytosis for cancer therapy. *Front Immunol* 2021;**12**:635173.
54. Stempels FC, Janssens MH, ter Beest M, Mesman RJ, Revelo NH, Ioannidis M, et al. Novel and conventional inhibitors of canonical autophagy differently affect LC3-associated phagocytosis. *FEBS Lett* 2022;**596**:491−509.

55. Vitale I, Manic G, Coussens LM, Kroemer G, Galluzzi L. Macrophages and metabolism in the tumor microenvironment. *Cell Metab* 2019;**30**:36−50.
56. Zhou XF, Liu XR, Huang L. Macrophage-mediated tumor cell phagocytosis: opportunity for nanomedicine intervention. *Adv Funct Mater* 2021;**31**:18.
57. Yang Q, Guo N, Zhou Y, Chen J, Wei Q, Han M. The role of tumor-associated macrophages (TAMs) in tumor progression and relevant advance in targeted therapy. *Acta Pharm Sin B* 2020;**10**:2156−70.
58. Lerbs T, Cui L, King ME, Chai T, Muscat C, Chung L, et al. CD47 prevents the elimination of diseased fibroblasts in scleroderma. *Jci Insight* 2020;**5**:e140458.
59. Pustulka SM, Ling K, Pish SL, Champion JA. Protein nanoparticle charge and hydrophobicity govern protein corona and macrophage uptake. *ACS Appl Mater Interfaces* 2020;**12**:48284−95.
60. Wang JF, Zhou XF, Wang HF, Xiao Q, Ding KF, Dong X, et al. Autophagy-inhibiting polymer as an effective nonviral cancer gene therapy vector with inherent apoptosis-sensitizing ability. *Biomaterials* 2020;**255**:120156.
61. Park EJ, Min KJ, Choi KS, Kubatka P, Kruzliak P, Kim DE, et al. Chloroquine enhances TRAIL-mediated apoptosis through up-regulation of DR5 by stabilization of mRNA and protein in cancer cells. *Sci Rep* 2016;**6**:22921.
62. Moore BR, Page-Sharp M, Stoney JR, Ilett KF, Jago JD, Batty KT. Pharmacokinetics, pharmacodynamics, and allometric scaling of chloroquine in a murine malaria model. *Antimicrob Agents Chemother* 2011;**55**:3899−907.
63. Wang H, Bai H, Wang J, Zhou X, Chen H, Wang L, et al. Nanoprodrug ratiometrically integrating autophagy inhibitor and genotoxic agent for treatment of triple-negative breast cancer. *Biomaterials* 2022;**283**:121458.